EUROPEAN LABORATORY FOR PARTICLE PHYSICS

CERN-PPE/96-162
20 November, 1996

A Measurement of $|V_{cb}|$ Using $\overline{\mathrm{B}}^0 \to \mathrm{D}^{*+}\ell^-\overline{\nu}_\ell$ Decays

The OPAL Collaboration

Abstract

We report a measurement of the Cabibbo-Kobayashi-Maskawa matrix element $|V_{cb}|$. From approximately 4.2 million hadronic Z^0 decays recorded with the OPAL detector, a sample is selected containing 1251 ± 125 $\overline{\mathrm{B}}^0 \to \mathrm{D}^{*+}\ell^-\overline{\nu}_\ell$ candidates, where ℓ is either an electron or a muon. Using Heavy Quark Effective Theory calculations for the decay form factor at zero recoil of the D^{*+} meson in the $\overline{\mathrm{B}}^0$ rest frame, we derive

$$|V_{cb}| = [36.0 \pm 2.1\,(\mathrm{stat}) \pm 2.4\,(\mathrm{syst}) \pm 1.2\,(\mathrm{theory})] \times 10^{-3}.$$

(submitted to Phys. Lett. **B**)

The OPAL Collaboration

K. Ackerstaff[8], G. Alexander[23], J. Allison[16], N. Altekamp[5], K. Ametewee[25], K.J. Anderson[9], S. Anderson[12], S. Arcelli[2], S. Asai[24], D. Axen[29], G. Azuelos[18,a], A.H. Ball[17], E. Barberio[8], R.J. Barlow[16], R. Bartoldus[3], J.R. Batley[5], J. Bechtluft[14], C. Beeston[16], T. Behnke[8], A.N. Bell[1], K.W. Bell[20], G. Bella[23], S. Bentvelsen[8], P. Berlich[10], S. Bethke[14], O. Biebel[14], A. Biguzzi[2], V. Blobel[27], I.J. Bloodworth[1], J.E. Bloomer[1], M. Bobinski[10], P. Bock[11], H.M. Bosch[11], M. Boutemeur[34], B.T. Bouwens[12], S. Braibant[12], R.M. Brown[20], H.J. Burckhart[8], C. Burgard[8], R. Bürgin[10], P. Capiluppi[2], R.K. Carnegie[6], A.A. Carter[13], J.R. Carter[5], C.Y. Chang[17], D.G. Charlton[1,b], D. Chrisman[4], P.E.L. Clarke[15], I. Cohen[23], J.E. Conboy[15], O.C. Cooke[16], M. Cuffiani[2], S. Dado[22], C. Dallapiccola[17], G.M. Dallavalle[2], S. De Jong[12], L.A. del Pozo[8], K. Desch[3], M.S. Dixit[7], E. do Couto e Silva[12], M. Doucet[18], E. Duchovni[26], G. Duckeck[34], I.P. Duerdoth[16], J.E.G. Edwards[16], P.G. Estabrooks[6], H.G. Evans[9], M. Evans[13], F. Fabbri[2], P. Fath[11], F. Fiedler[27], M. Fierro[2], H.M. Fischer[3], R. Folman[26], D.G. Fong[17], M. Foucher[17], A. Fürtjes[8], P. Gagnon[7], A. Gaidot[21], J.W. Gary[4], J. Gascon[18], S.M. Gascon-Shotkin[17], N.I. Geddes[20], C. Geich-Gimbel[3], F.X. Gentit[21], T. Geralis[20], G. Giacomelli[2], P. Giacomelli[4], R. Giacomelli[2], V. Gibson[5], W.R. Gibson[13], D.M. Gingrich[30,a], D. Glenzinski[9], J. Goldberg[22], M.J. Goodrick[5], W. Gorn[4], C. Grandi[2], E. Gross[26], J. Grunhaus[23], M. Gruwé[8], C. Hajdu[32], G.G. Hanson[12], M. Hansroul[8], M. Hapke[13], C.K. Hargrove[7], P.A. Hart[9], C. Hartmann[3], M. Hauschild[8], C.M. Hawkes[5], R. Hawkings[8], R.J. Hemingway[6], M. Herndon[17], G. Herten[10], R.D. Heuer[8], M.D. Hildreth[8], J.C. Hill[5], S.J. Hillier[1], T. Hilse[10], P.R. Hobson[25], R.J. Homer[1], A.K. Honma[28,a], D. Horváth[32,c], R. Howard[29], R.E. Hughes-Jones[16], D.E. Hutchcroft[5], P. Igo-Kemenes[11], D.C. Imrie[25], M.R. Ingram[16], K. Ishii[24], A. Jawahery[17], P.W. Jeffreys[20], H. Jeremie[18], M. Jimack[1], A. Joly[18], C.R. Jones[5], G. Jones[16], M. Jones[6], R.W.L. Jones[8], U. Jost[11], P. Jovanovic[1], T.R. Junk[8], D. Karlen[6], K. Kawagoe[24], T. Kawamoto[24], R.K. Keeler[28], R.G. Kellogg[17], B.W. Kennedy[20], B.J. King[8], J. Kirk[29], S. Kluth[8], T. Kobayashi[24], M. Kobel[10], D.S. Koetke[6], T.P. Kokott[3], M. Kolrep[10], S. Komamiya[24], T. Kress[11], P. Krieger[6], J. von Krogh[11], P. Kyberd[13], G.D. Lafferty[16], H. Lafoux[21], R. Lahmann[17], W.P. Lai[19], D. Lanske[14], J. Lauber[15], S.R. Lautenschlager[31], J.G. Layter[4], D. Lazic[22], A.M. Lee[31], E. Lefebvre[18], D. Lellouch[26], J. Letts[2], L. Levinson[26], C. Lewis[15], S.L. Lloyd[13], F.K. Loebinger[16], G.D. Long[17], M.J. Losty[7], J. Ludwig[10], A. Malik[21], M. Mannelli[8], S. Marcellini[2], C. Markus[3], A.J. Martin[13], J.P. Martin[18], G. Martinez[17], T. Mashimo[24], W. Matthews[25], P. Mättig[3], W.J. McDonald[30], J. McKenna[29], E.A. Mckigney[15], T.J. McMahon[1], A.I. McNab[13], R.A. McPherson[8], F. Meijers[8], S. Menke[3], F.S. Merritt[9], H. Mes[7], J. Meyer[27], A. Michelini[2], G. Mikenberg[26], D.J. Miller[15], R. Mir[26], W. Mohr[10], A. Montanari[2], T. Mori[24], M. Morii[24], U. Müller[3], K. Nagai[26], I. Nakamura[24], H.A. Neal[8], B. Nellen[3], B. Nijjhar[16], R. Nisius[8], S.W. O'Neale[1], F.G. Oakham[7], F. Odorici[2], H.O. Ogren[12], N.J. Oldershaw[16], T. Omori[24], M.J. Oreglia[9], S. Orito[24], J. Pálinkás[33,d], G. Pásztor[32], J.R. Pater[16], G.N. Patrick[20], J. Patt[10], M.J. Pearce[1], S. Petzold[27], P. Pfeifenschneider[14], J.E. Pilcher[9], J. Pinfold[30], D.E. Plane[8], P. Poffenberger[28], B. Poli[2], A. Posthaus[3], H. Przysiezniak[30], D.L. Rees[1], D. Rigby[1], S. Robertson[28], S.A. Robins[13], N. Rodning[30], J.M. Roney[28], A. Rooke[15], E. Ros[8], A.M. Rossi[2], M. Rosvick[28], P. Routenburg[30], Y. Rozen[22], K. Runge[10], O. Runolfsson[8], U. Ruppel[14], D.R. Rust[12], R. Rylko[25], K. Sachs[10], E.K.G. Sarkisyan[23], M. Sasaki[24], C. Sbarra[2], A.D. Schaile[34], O. Schaile[34], F. Scharf[3], P. Scharff-Hansen[8], P.. Schenk[27], B. Schmitt[8], S. Schmitt[11], M. Schröder[8], H.C. Schultz-Coulon[10], M. Schulz[8], M. Schumacher[3], P. Schütz[3], W.G. Scott[20], T.G. Shears[16], B.C. Shen[4], C.H. Shepherd-Themistocleous[8], P. Sherwood[15], G.P. Siroli[2], A. Sittler[27], A. Skillman[15], A. Skuja[17], A.M. Smith[8], T.J. Smith[28], G.A. Snow[17], R. Sobie[28], S. Söldner-Rembold[10], R.W. Springer[30],

M. Sproston[20], A. Stahl[3], M. Steiert[11], K. Stephens[16], J. Steuerer[27], B. Stockhausen[3], D. Strom[19], F. Strumia[8], P. Szymanski[20], R. Tafirout[18], S.D. Talbot[1], S. Tanaka[24], P. Taras[18], S. Tarem[22], M. Thiergen[10], M.A. Thomson[8], E. von Törne[3], S. Towers[6], I. Trigger[18], T. Tsukamoto[24], E. Tsur[23], A.S. Turcot[9], M.F. Turner-Watson[8], P. Utzat[11], R. Van Kooten[12], G. Vasseur[21], M. Verzocchi[10], P. Vikas[18], M. Vincter[28], E.H. Vokurka[16], F. Wäckerle[10], A. Wagner[27], C.P. Ward[5], D.R. Ward[5], J.J. Ward[15], P.M. Watkins[1], A.T. Watson[1], N.K. Watson[7], P.S. Wells[8], N. Wermes[3], J.S. White[28], B.. Wilkens[10], G.W. Wilson[27], J.A. Wilson[1], G. Wolf[26], S. Wotton[5], T.R. Wyatt[16], S. Yamashita[24], G. Yekutieli[26], V. Zacek[18]

[1]School of Physics and Space Research, University of Birmingham, Birmingham B15 2TT, UK
[2]Dipartimento di Fisica dell' Università di Bologna and INFN, I-40126 Bologna, Italy
[3]Physikalisches Institut, Universität Bonn, D-53115 Bonn, Germany
[4]Department of Physics, University of California, Riverside CA 92521, USA
[5]Cavendish Laboratory, Cambridge CB3 0HE, UK
[6] Ottawa-Carleton Institute for Physics, Department of Physics, Carleton University, Ottawa, Ontario K1S 5B6, Canada
[7]Centre for Research in Particle Physics, Carleton University, Ottawa, Ontario K1S 5B6, Canada
[8]CERN, European Organisation for Particle Physics, CH-1211 Geneva 23, Switzerland
[9]Enrico Fermi Institute and Department of Physics, University of Chicago, Chicago IL 60637, USA
[10]Fakultät für Physik, Albert Ludwigs Universität, D-79104 Freiburg, Germany
[11]Physikalisches Institut, Universität Heidelberg, D-69120 Heidelberg, Germany
[12]Indiana University, Department of Physics, Swain Hall West 117, Bloomington IN 47405, USA
[13]Queen Mary and Westfield College, University of London, London E1 4NS, UK
[14]Technische Hochschule Aachen, III Physikalisches Institut, Sommerfeldstrasse 26-28, D-52056 Aachen, Germany
[15]University College London, London WC1E 6BT, UK
[16]Department of Physics, Schuster Laboratory, The University, Manchester M13 9PL, UK
[17]Department of Physics, University of Maryland, College Park, MD 20742, USA
[18]Laboratoire de Physique Nucléaire, Université de Montréal, Montréal, Quebec H3C 3J7, Canada
[19]University of Oregon, Department of Physics, Eugene OR 97403, USA
[20]Rutherford Appleton Laboratory, Chilton, Didcot, Oxfordshire OX11 0QX, UK
[21]CEA, DAPNIA/SPP, CE-Saclay, F-91191 Gif-sur-Yvette, France
[22]Department of Physics, Technion-Israel Institute of Technology, Haifa 32000, Israel
[23]Department of Physics and Astronomy, Tel Aviv University, Tel Aviv 69978, Israel
[24]International Centre for Elementary Particle Physics and Department of Physics, University of Tokyo, Tokyo 113, and Kobe University, Kobe 657, Japan
[25]Brunel University, Uxbridge, Middlesex UB8 3PH, UK
[26]Particle Physics Department, Weizmann Institute of Science, Rehovot 76100, Israel
[27]Universität Hamburg/DESY, II Institut für Experimental Physik, Notkestrasse 85, D-22607 Hamburg, Germany
[28]University of Victoria, Department of Physics, P O Box 3055, Victoria BC V8W 3P6, Canada
[29]University of British Columbia, Department of Physics, Vancouver BC V6T 1Z1, Canada
[30]University of Alberta, Department of Physics, Edmonton AB T6G 2J1, Canada
[31]Duke University, Dept of Physics, Durham, NC 27708-0305, USA

[32]Research Institute for Particle and Nuclear Physics, H-1525 Budapest, P O Box 49, Hungary
[33]Institute of Nuclear Research, H-4001 Debrecen, P O Box 51, Hungary
[34]Ludwigs-Maximilians-Universität München, Sektion Physik, Am Coulombwall 1, D-85748 Garching, Germany

[a] and at TRIUMF, Vancouver, Canada V6T 2A3
[b] and Royal Society University Research Fellow
[c] and Institute of Nuclear Research, Debrecen, Hungary
[d] and Department of Experimental Physics, Lajos Kossuth University, Debrecen, Hungary

1 Introduction

In the framework of the Standard Model of electroweak interactions, the elements of the Cabibbo-Kobayashi-Maskawa mixing matrix are free parameters, constrained by the unitarity of the matrix, which can only be determined experimentally. Until recently, the element $|V_{\mathrm{cb}}|$ was extracted from measurements of the lifetime and inclusive semileptonic branching fraction of the B meson [1]. The theoretical uncertainties are large, owing to the presence of the b and c quark masses in the theoretical calculations of the inclusive decay rate as well as the uncertainties in the perturbative QCD corrections [2]. Recent developments in Heavy Quark Effective Theory (HQET) [3] provide a means to determine $|V_{\mathrm{cb}}|$, with relatively small theoretical uncertainties, by studying the decay rate of the exclusive semileptonic decay[1] $\overline{\mathrm{B}}^0 \to \mathrm{D}^{*+}\ell^-\overline{\nu}_\ell$ as a function of the recoil kinematics of the D^{*+} meson [4]-[7]. The decay rate is parameterized as a function of the variable ω, the product of the four velocities of the D^{*+} and the $\overline{\mathrm{B}}^0$, which is related to the square of the four momentum transfer from the $\overline{\mathrm{B}}^0$ to the $\ell^-\overline{\nu}_\ell$ system, q^2,

$$\omega = \frac{m^2_{\mathrm{D}^{*+}} + m^2_{\mathrm{B}^0} - q^2}{2m_{\mathrm{B}^0}m_{\mathrm{D}^{*+}}},$$

and ranges from 1.0, when the D^{*+} is produced at rest in the $\overline{\mathrm{B}}^0$ rest frame, to about 1.50. Using HQET, the differential partial width for this decay is given by

$$\begin{aligned} \frac{\mathrm{d}\Gamma}{\mathrm{d}\omega} &= \frac{1}{\tau_{\mathrm{B}^0}} \frac{\mathrm{d}Br\left(\overline{\mathrm{B}}^0 \to \mathrm{D}^{*+}\ell^-\overline{\nu}_\ell\right)}{\mathrm{d}\omega} \qquad (1) \\ &= \frac{G_\mathrm{F}^2}{48\pi^3} m^3_{\mathrm{D}^{*+}} \left(m_{\mathrm{B}^0} - m_{\mathrm{D}^{*+}}\right)^2 \mathcal{F}^2(\omega) \left|V_{\mathrm{cb}}\right|^2 \\ &\quad \times\sqrt{\omega^2-1}\left[4\omega(\omega+1)\frac{1-2\omega r + r^2}{(1-r)^2} + (\omega+1)^2\right], \end{aligned}$$

where $r = m_{\mathrm{D}^{*+}}/m_{\mathrm{B}^0}$ and $\mathcal{F}(\omega)$ is the hadronic form factor for the decay [7]. Although the shape of this form factor is not known, its magnitude at zero recoil, $\omega = 1$, can be estimated using

[1]In this paper, ℓ will refer to either an electron or a muon, and charge conjugate reactions are always implied. We also use the convention $\hbar = c = 1$.

HQET. In the heavy quark limit ($m_b \to \infty$), $\mathcal{F}(\omega)$ coincides with the Isgur-Wise function [5, 6] which is normalized to unity at the point of zero recoil. Corrections to $\mathcal{F}(1)$ have been calculated to take into account the effect of finite quark masses and QCD corrections [8]. Calculations of these corrections yield $\mathcal{F}(1) = 0.91 \pm 0.03$ [9]. Thus, an accurate determination of $\mathcal{F}(1)|V_{cb}|$ can be made by measuring $\mathrm{d}\Gamma/\mathrm{d}\omega$ and extrapolating to $\omega = 1$, with $\mathcal{F}(\omega)$ approximated by a power series expansion around $\omega = 1$. Since the decay rate vanishes at $\omega = 1$, the accuracy of the extrapolation relies on achieving a reasonably constant reconstruction efficiency in the region about $\omega = 1$.

Previous measurements of $|V_{cb}|$ have been made, using this method, at the $\Upsilon(4S)$ [10, 11] and at LEP [12, 13]. These are currently the most accurate measurements of $|V_{cb}|$, for which the overall statistical and systematic uncertainties are around $7-10\%$ and the theoretical errors are only of the order of 3%.

2 The OPAL Detector

The OPAL detector has been described elsewhere [14, 15]. Tracking of charged particles is performed by a central detector, consisting of a silicon microvertex detector, a vertex chamber, a jet chamber and z-chambers.[2] The central detector is positioned inside a solenoid, which provides a uniform magnetic field of 0.435 T. The silicon microvertex detector consists of two layers of silicon strip detectors; the inner layer covers a polar angle range of $|\cos\theta| < 0.83$ and the outer layer covers $|\cos\theta| < 0.77$. This detector provided both ϕ- and z-coordinates for data taken in 1993-1995, but ϕ-coordinates only for 1991 and 1992. Only ϕ-coordinate information was used in this analysis. The vertex chamber is a precision drift chamber which covers the range $|\cos\theta| < 0.95$. The jet chamber is a large-volume drift chamber, 4 m long and 3.7 m in diameter, providing both tracking and $\mathrm{d}E/\mathrm{d}x$ information. The z-chambers measure the z-coordinate of tracks as they leave the jet chamber in the range $|\cos\theta| < 0.72$. The coil is surrounded by a time-of-flight counter array and a lead-glass electromagnetic calorimeter with a presampler. The lead-glass blocks cover the range $|\cos\theta| < 0.98$. The magnet return yoke is instrumented with streamer tubes and serves as a hadron calorimeter. Outside the hadron calorimeter are muon chambers, which cover 93% of the full solid angle.

3 Event Selection and $\mathrm{D}^{*+}\ell^-$ Reconstruction

The data sample used in this analysis consists of about 4.2 million hadronic Z^0 decays collected during the period 1990-1995, at center-of-mass energies in the vicinity of the Z^0 resonance. The selection of hadronic Z^0 decays is described in [16]. Charged tracks and electromagnetic clusters unassociated with any charged track are grouped into jets using the JADE E0 recombination

[2]The coordinate system is defined with positive z along the e^- beam direction, θ and ϕ being the polar and azimuthal angles. The origin is taken to be the center of the detector.

scheme with a $y_{\rm cut}$ value of 0.04 [17].

Simulated event samples were generated using the JETSET 7.4 Monte Carlo program [18], together with a program to simulate the response of the OPAL detector [19]. The Monte Carlo samples used include approximately 4 million simulated multihadronic Z^0 decays and one million $Z^0 \to b\overline{b}$ decays (the equivalent of about 4.5 million multihadronic decays). In addition, special high statistics Monte Carlo samples containing at least one B^0 which decayed into the decay products of interest, as described below, were generated. These samples correspond to more than 12 million multihadronic Z^0 decays.

Candidates for the exclusive decay $\overline{B}^0 \to D^{*+}\ell^-\overline{\nu}_\ell$ are selected from events where a D^{*+} and a lepton of opposite charge are found in the same jet. An artificial neural network is used to identify electrons [20], and photon conversions are rejected as described in [21]. Muons are selected as described in [22]. Electrons are required to have momentum greater than 2 GeV and muons to have momentum above 3 GeV. The lepton is required to have momentum component greater than 0.6 GeV transverse to the jet axis, where the jet definition includes the lepton.

The D^{*+} candidates are reconstructed in the decay chains

$$\begin{array}{lll} D^{*+} \to D^0\pi^+ & & \\ \quad\hookrightarrow K^-\pi^+ & \text{“3-prong”}, \\ \quad\hookrightarrow K^-\pi^+\pi^0 & \text{“satellite”}, \end{array}$$

where no attempt is made to reconstruct the π^0 in the satellite mode. Since the D^0 is not fully reconstructed in this mode, it gives rise to a broad peak in the $K^-\pi^+$ invariant mass spectrum about 250 MeV below the D^0 mass [23]. The slow pion from the D^{*+} decay carries most of the information about the D^{*+} momentum in the laboratory frame, and so it can be used to estimate the D^{*+} momentum for the satellite events. Assuming that it is produced at rest in the D^{*+} rest frame and follows the D^{*+} direction, the slow pion momentum, $\vec{p}_s$, can be used to reconstruct the D^{*+} momentum, $\vec{p}_{D^*}$, to a good approximation by $\vec{p}_{D^*} = \vec{p}_s\, m_{D^*}/m_\pi$, where m_{D^*} is the mass of the D^{*+} and m_π is the pion mass. The accuracy of this method has been studied in Monte Carlo simulated samples and by applying the method to fully reconstructed 3-prong candidates [24]. These studies show that the D^{*+} momentum obtained in this way introduces no systematic shift and yields a resolution of about 15%.

The tracks forming the D^{*+} candidate are required to be in the same jet and to pass a set of quality cuts: $|d_0| < 0.5$ cm; $|z_0| < 20$ cm; $p_{xy} > 0.25$ GeV; and at least 40 hits in the jet chamber, where d_0 is the measured distance of closest approach to the nominal e^+e^- interaction point in the x-y plane, z_0 is the z position at that point and p_{xy} is the momentum component in the x-y plane. The lepton tracks are also required to pass the above quality cuts.

In order to reduce combinatorial background, the tracks forming the D^{*+} candidate are subject to particle identification cuts. For candidate pion tracks, the probability for the measured $\mathrm{d}E/\mathrm{d}x$ value to be consistent with the pion hypothesis is required to be greater than 1%. For candidate kaon tracks, the probability for the kaon hypothesis is required to be greater than 1%. For the satellite channel this requirement is tightened to 5% if the measured $\mathrm{d}E/\mathrm{d}x$ is greater than the expected value. This requirement reduces the background from pion tracks, for which the mean $\mathrm{d}E/\mathrm{d}x$ value is above that of kaons. We require that x_{D^*}, the visible D^{*+} energy scaled by the beam energy, be greater than 0.15 for the 3-prong mode and greater than 0.20 for the satellite mode.

The primary event vertex is reconstructed using all the charged tracks in the event, except the lepton track and those forming the D^{*+}, along with knowledge of the current average position and effective spread of the $\mathrm{e}^+\mathrm{e}^-$ collision point. In this process, tracks that are significantly separated from the primary vertex position are excluded from the final primary vertex reconstruction.

The D^0 vertex is reconstructed by fitting in the x-y plane the three tracks forming the D^{*+} candidate. The slow pion track from the D^{*+} decay is included in the vertex fit since its direction follows closely that of the D^0 and so can be used to constrain the D^0 direction. The $\overline{\mathrm{B}}^0$ vertex is then formed by extrapolating, in the x-y plane, the D^{*+} momentum vector from the D^0 vertex back to the intersection with the lepton track. The projection of the $\overline{\mathrm{B}}^0$ decay length in the x-y plane, L, is determined from a fit to the primary vertex and the reconstructed $\overline{\mathrm{B}}^0$ vertex using the direction of the $\mathrm{D}^{*+}\ell^-$ momentum vector as a constraint. It is signed negative if the $\overline{\mathrm{B}}^0$ vertex lies on the opposite side of the primary vertex from the D^0 vertex. We require that L be greater than -1 cm and that the error on L, σ_L, be less than 1 cm. L is signed negative if the $\mathrm{D}^{*+}\ell^-$ intersection point lies on the opposite side of the primary vertex to the D^{*+} decay vertex.

We select $\mathrm{D}^{*+}\ell^-$ candidates in the following mass windows: $\mathrm{K}^-\pi^+$ invariant mass, $M(\mathrm{K}^-\pi^+)$, in the range 1.785-1.945 GeV for the 3-prong mode and 1.425-1.750 GeV for the satellite mode; $\mathrm{D}^{*+} - \mathrm{D}^0$ mass difference, δ_M, in the range $\delta_M < 0.149$ GeV for 3-prong candidates and $\delta_M < 0.157$ GeV for satellite candidates; and $\mathrm{D}^{*+}\ell^-$ invariant mass in the range 2.8-5.3 GeV for both 3-prong and satellite candidates.

Figure 1 shows the distribution of the mass difference between the D^{*+} candidate and the D^0 candidate for selected $\mathrm{D}^{*+}\ell^-$ candidates, with all cuts applied except those on δ_M. There are a total of 814 3-prong and 1369 satellite candidates in the signal regions.

The shape of the combinatorial background for δ_M is determined from the data using a reflected soft pion technique [24]. It makes use of a background sample consisting of reflected pion candidates, reconstructed by selecting a slow pion candidate track from the hemisphere opposite a normal D^0 candidate. The D^{*+} candidate is formed after reflecting the slow pion through the origin. Reflected pions of either charge are used. Monte Carlo studies show that this sample describes well the shape of the combinatorial background below the signal [24]. The shape is parameterized from a fit to the resulting δ_M distribution using the empirical form:

$$A\, e^{-B\,\delta_M} \left(\frac{\delta_M}{m_\pi} - 1\right)^C , \tag{2}$$

where m_π is the pion mass and A, B and C are free fit parameters. The amount of combinatorial background in the $\mathrm{D}^{*+}\ell^-$ sample is found by fixing B and C to the values obtained from the background sample fit and fitting A in the region $0.17 < \delta_M < 0.23$ GeV for the 3-prong mode. For the satellite mode, A is fitted in the region $0.18 < \delta_M < 0.23$ GeV, to avoid including for the longer tail of the signal. We estimate 147 ± 14 and 355 ± 21 combinatorial background events for the 3-prong and satellite modes, respectively.

4 Reconstruction of ω

The quantity ω is reconstructed for each candidate from the reconstructed $D^{*+}\ell^-$ and event kinematics. In a coordinate system where the z-axis coincides with the direction of the $D^{*+}\ell^-$ momentum and the y-axis is chosen to be in the direction of the vector product of the D^{*+} and lepton momenta, ω is expressed as

$$\omega = \frac{m_{B^0}^2 + m_{D^{*+}}^2 - m_\ell^2 - 2E_\nu E_\ell + 2E_\nu p_\ell \cos\theta_\nu \cos\theta_\ell + 2E_\nu p_\ell \sin\theta_\ell \sin\theta_\nu \cos\phi_\nu}{2m_{B^0} m_{D^{*+}}},$$

where m_ℓ, p_ℓ and E_ℓ are the mass, momentum and energy of the lepton and E_ν is the energy of the missing neutrino. The variable ϕ_ν is the azimuthal angle of the neutrino vector and θ_ℓ and θ_ν are the polar angles of the lepton and neutrino, respectively. The estimation of these quantities is described below.

The Neutrino Energy: The neutrino energy is estimated using a technique which treats the whole event as a two-body decay of a Z^0 at rest [25]. By energy and momentum conservation,

$$E_1 = \frac{M_{Z^0}^2 + m_1^2 - m_2^2}{2M_{Z^0}},$$

where E_1 and m_1 are the energy and mass of the first body and m_2 is the mass of the other body. We take m_1 to be the mass of the jet containing the $D^{*+}\ell^-$ and approximate it to be the B^0 mass, 5.279 GeV (the result is insensitive to this assumption). The mass of the rest of the event, m_2, is calculated by summing over those tracks and unassociated electromagnetic clusters which are not included in the $D^{*+}\ell^-$ jet. We assume all charged tracks are pions and all clusters are photons. The neutrino energy is defined by the relation $E_\nu = E_1 - E_{vis1}$, where E_{vis1} is the visible energy in the jet, obtained by summing over the tracks and unassociated clusters. We reject events for which $E_\nu < 0$. Approximately 10% of the events fail this criterion. The resolution on the reconstructed neutrino energy has an r.m.s. of about 2.7 GeV for the 3-prong decay mode and about 2.8 GeV for the satellite mode, and no significant bias in the reconstructed E_ν is observed. The average neutrino energy for the signal process is about 8 GeV and has an r.m.s. spread of 5 GeV.

The Neutrino Polar Angle: The angle θ_ν is calculated from the constraint $m_{B^0}^2 = M_{D^*\ell\overline{\nu}}^2$:

$$\cos\theta_\nu = \frac{E_{D^*\ell}}{P_{D^*\ell}} - \frac{m_{B^0}^2 - M_{D^*\ell}^2}{2P_{D^*\ell}E_\nu}, \tag{3}$$

where $M_{D^*\ell}$, $P_{D^*\ell}$ and $E_{D^*\ell}$ are the mass, momentum and energy of the $D^{*+}\ell^-$ candidate. If the calculated value of $\cos\theta_\nu$ is unphysical the event is rejected. This occurs for only $\sim 5\%$

of the candidates. The resolution on θ_ν is approximately $3°$ for both the 3-prong and satellite modes.

The Neutrino Azimuthal Angle: The azimuthal direction of the neutrino is reconstructed in two different ways, depending on the quality of the estimated $\overline{\mathrm{B}}^0$ vertex. If the χ^2 of the vertex fit is less than 15 and the $\overline{\mathrm{B}}^0$ decay length is greater than 1 mm, which is true for $\sim 30\%$ of the events, the $\overline{\mathrm{B}}^0$ flight direction is estimated as the vector between the primary vertex and the $\mathrm{D}^{*+}\ell^-$ vertex.

If these cuts are not satisfied, we use the missing energy in the event to estimate ϕ_ν, as follows. The visible momentum in the event, $\vec{P}_{vis}$, is calculated using a global corrected energy algorithm [26]:

$$\vec{P}_{vis} = \sum_i \vec{p}_{trk,i} + \sum_j \vec{p}_{cal,j} - \sum_k \vec{f}_k(p_{trk,k}),$$

where the first term is the sum of charged track momenta, the second term is the sum of electromagnetic and hadronic cluster momenta and the third term is a sum of corrections for each track. The corrections take into account the fact that charged particles are measured in the tracking chambers as well as in the electromagnetic and hadron calorimeters, so momenta must be subtracted from the first two terms in order to avoid double counting. Each track is identified as being either an electron, a muon or a pion (all non-leptons are considered to be pions). Lepton identification is performed as described in section 3. The amount of energy the track is expected to deposit in the calorimeters is then estimated, according to the assigned particle type, and is included in the correction term. The missing momentum is $-\vec{P}_{vis}$, the momentum vector which balances the total momentum to zero. The sum of the missing momentum and the momentum of the jet containing the $\mathrm{D}^{*+}\ell^-$ candidate gives an estimate of the $\overline{\mathrm{B}}^0$ direction. For instances in which $-\vec{P}_{vis}$ is greater than $90°$ from the $\mathrm{D}^{*+}\ell^-$ jet direction, we use the jet direction as the $\overline{\mathrm{B}}^0$ direction. This occurs for approximately 15% of the candidates.

The estimated direction of the B^0 is combined with the estimate of E_{B^0}, defined by $E_{\mathrm{B}^0} = E_{\mathrm{D}^*\ell} + E_\nu$, and the $\overline{\mathrm{B}}^0$ mass, 5.279 GeV, to determine the $\overline{\mathrm{B}}^0$ momentum vector, $\vec{p}_{\mathrm{B}^0}$. The direction of the neutrino vector is given by $\vec{p}_\nu = \vec{p}_{\mathrm{B}^0} - \vec{p}_{\mathrm{D}^*\ell}$. From this vector we derive the azimuthal angle ϕ_ν. The resolution on ϕ_ν is approximately $30°$, which dominates the overall ω resolution. The polar angle θ_ν is estimated with much greater accuracy using equation 3 than is possible by using the missing energy direction.

Figure 2 shows plots of the true ω versus the reconstructed value, for Monte Carlo simulated $\overline{\mathrm{B}}^0 \to \mathrm{D}^{*+}\ell^-\overline{\nu}_\ell$ events for the 3-prong and satellite modes. The ω resolution is obtained by fitting the distributions of true ω versus reconstructed ω with a Gaussian function for five different ranges of true ω. The variations of the fitted widths in the different ranges are of the order of (5-10)%. These widths are averaged, weighting by the number of events in each range, to obtain mean overall resolutions of 0.10 and 0.12 for the 3-prong and satellite decays, respectively.

5 The Signal and Background Fractions

In addition to the signal process, various background processes contribute to the selected events. The amount of each background is estimated using previously measured branching fractions and selection efficiencies calculated from Monte Carlo simulated events. Table 1 lists the branching fractions used in the rest of this section.

The largest background is from the decays $\mathrm{B}^- \to \mathrm{D}^{*+}\pi^-\ell^-\overline{\nu}_\ell\mathrm{X}$, $\overline{\mathrm{B}}^0 \to \mathrm{D}^{*+}\pi^0\ell^-\overline{\nu}_\ell\mathrm{X}$ and $\overline{\mathrm{B}}^0_\mathrm{s} \to \mathrm{D}^{*+}\mathrm{K}^0\ell^-\overline{\nu}_\ell\mathrm{X}$, which are expected to be dominated by resonant D^{**} decays. Isospin and SU(3) flavor symmetry are used to relate the branching fractions for the $\overline{\mathrm{B}}^0$ and $\overline{\mathrm{B}}^0_\mathrm{s}$ decays to the measured rate of $\mathrm{b} \to \mathrm{D}^{*+}\pi^-\ell^-\overline{\nu}_\ell\mathrm{X}$ [27]. We assume $f(\mathrm{b}\to\mathrm{B}^-) = f(\mathrm{b}\to\overline{\mathrm{B}}^0)$ and $f(\mathrm{b}\to\overline{\mathrm{B}}^0_\mathrm{s}) = (11.2\pm1.8)\%$ [28]. For the rest of this paper, we use the notation $\overline{\mathrm{B}} \to \mathrm{D}^{*+}\mathrm{h}\ell^-\overline{\nu}_\ell$ to refer to the sum of the $\overline{\mathrm{B}}^0$, B^- and $\overline{\mathrm{B}}^0_\mathrm{s}$ decay modes mentioned above.

Process	Branching Fraction (%)	Reference
$R_\mathrm{b} = \Gamma_{\mathrm{b}\overline{\mathrm{b}}}/\Gamma_\mathrm{had}$	22.06 ± 0.21	[29]
$f(\mathrm{b}\to\overline{\mathrm{B}}^0)$	37.8 ± 2.2	[28]
$f(\mathrm{b}\to\overline{\mathrm{B}}^0_\mathrm{s})$	11.2 ± 1.8	[28]
$Br(\mathrm{b}\to\mathrm{D}^{*+}\pi^-\ell^-\overline{\nu}_\ell\mathrm{X})$	0.37 ± 0.12	[27]
$Br(\mathrm{b}\to\mathrm{D}^{*+}\tau^-\overline{\nu}_\tau\mathrm{X})$	2.06 ± 0.36	[30]
$Br(\overline{\mathrm{B}}^0\to\mathrm{D}^{*+}\mathrm{D}_\mathrm{s}^{(*)-}\mathrm{X})$	4.3 ± 1.2	[28]
$Br(\mathrm{D}^{*+}\to\mathrm{D}^0\pi^+)$	68.1 ± 1.3	[28]
$Br(\mathrm{D}^0\to\mathrm{K}^-\pi^+)$	3.83 ± 0.12	[28]
$Br(\mathrm{D}^0\to\mathrm{K}^-\pi^+\pi^0)$	13.9 ± 0.9	[28]

Table 1: The branching fractions used in calculating the background in the $\mathrm{D}^{*+}\ell^-$ sample.

The largest backgrounds after accounting for the $\overline{\mathrm{B}} \to \mathrm{D}^{*+}\mathrm{h}\ell^-\overline{\nu}_\ell$ decays are events of the type $\overline{\mathrm{B}}^0 \to \mathrm{D}^{*+}\mathrm{D}_\mathrm{s}^{(*)-}\mathrm{X}$, with the D_s^- decaying semileptonically, and $\mathrm{b}\to\mathrm{D}^{*+}\tau^-\overline{\nu}_\tau\mathrm{X}$, with the τ decaying leptonically. The amount of background from the former process is estimated using the measured $Br(\overline{\mathrm{B}}^0 \to \mathrm{D}^{*+}\mathrm{D}_\mathrm{s}^{(*)-}\mathrm{X})$ [28] and assuming that the inclusive semileptonic decay rate of the D_s^- meson is the same as that of the D^0 [28]. The amount of background from the process $\mathrm{b}\to\mathrm{D}^{*+}\tau^-\overline{\nu}_\tau$ is estimated using the measured inclusive $\mathrm{b}\to\tau^-\mathrm{X}$ branching fraction [30] along with the branching fraction for leptonic τ^- decays [28]. We assume that 75% of the inclusive decays to a τ^- involve a D^{*+}.

The combinatorial background is estimated from the fits to the δ_M distributions, as described in section 3. This gives the contribution from random combinations of tracks forming D^{*+} candidates. There are additional contributions from fake lepton candidates and misidentified, so called fake, D^0 decays. The fake lepton component is estimated from the excess of events in the wrong charge δ_M distribution (D^{*+} and lepton having the same charge) after subtracting the estimated random background using the shape parameterization given by equation 2. We estimate 9 ± 4 and 11 ± 5 background events of this type for the 3-prong and satellite modes, respectively, which are consistent with the predictions from Monte Carlo simulations. The fake D^0 background is characterized by events in which the slow pion from the D^{*+} decay is correctly identified, but the D^0 decay mode is misidentified. These events produce an enhancement in the δ_M spectrum, but do not display peaks in the relevant reconstructed D^0 mass regions. Therefore, the fake D^0 background can be estimated by making a selection of candidates identical to that for signal events, except that no $\mathrm{K}^-\pi^+$ invariant mass cut is used and only candidates in the signal region of the δ_M distribution are accepted. The number of fake D^0 events is taken as the difference between the combinatorial background determined from the $\mathrm{K}^-\pi^+$ invariant mass distribution and that calculated from the δ_M distribution. We estimate a total of 16 ± 6 fake D^0 in the 3-prong events and 58 ± 15 in the satellite events.

Table 2 lists the estimated number of signal and background events in the selected $\mathrm{D}^{*+}\ell^-$ samples.

Component	Number of Events 3-prong	Satellite
Total Candidates	814	1396
$\overline{\mathrm{B}} \to \mathrm{D}^{*+}\mathrm{h}\ell^-\overline{\nu}_\ell$	119 ± 40	191 ± 66
$\overline{\mathrm{B}}^0 \to \mathrm{D}^{*+}\tau^-\overline{\nu}_\tau$	14 ± 4	20 ± 6
$\overline{\mathrm{B}}^0 \to \mathrm{D}^{*+}\mathrm{D}_\mathrm{s}^{(*)-}$	7 ± 2	12 ± 3
Combinatorial Background	147 ± 14	355 ± 21
Fake Leptons	9 ± 4	11 ± 5
Fake D^0	16 ± 6	58 ± 15
$\overline{\mathrm{B}}^0 \to \mathrm{D}^{*+}\ell^-\overline{\nu}_\ell$	502 ± 44	749 ± 72

Table 2: The estimated number of signal and background events in the selected $\mathrm{D}^{*+}\ell^-$ sample. The quoted uncertainties on the number of signal events include only the errors on the number of background events.

6 The Fit for $\mathcal{F}(1)|V_{\mathrm{cb}}|$

We measure $\mathcal{F}(1)|V_{\mathrm{cb}}|$ from the ω spectrum using an unbinned maximum likelihood fit. Each event i is assigned a probability density which is a sum of signal and background terms:

$$\mathcal{P}^k(\omega_i) = \frac{N_s^k}{N^k}\mathcal{P}_s^k(\omega_i) + \frac{(N^k - N_s^k)}{N^k}\sum_j f_j^k \mathcal{P}_j^k(\omega_i),$$

where ω_i is the measured value of ω for candidate i, $\mathcal{P}_s^k$ is the probability density function for the signal process (where the superscript k refers to the sample the candidate belongs to:

3-prong or satellite), $\mathcal{P}_j^k$ is the probability density function for background process j (j is any of the backgrounds listed in Table 2), N^k is the total number of selected candidates, N_s^k is the estimated number of signal events and f_j^k is the fraction of background process j relative to the total background ($\sum_j f_j^k = 1$).

The probability density function for the signal is derived from equation 1, which can be rewritten as

$$\frac{\mathrm{d}\Gamma}{\mathrm{d}\omega} = \mathcal{K}(\omega)\mathcal{F}^2(\omega)|V_{\mathrm{cb}}|^2,$$

where all of the known quantities have been collected into a single function,

$$\mathcal{K}(\omega) = \frac{G_{\mathrm{F}}^2}{48\pi^3} m_{\mathrm{D}^{*+}}^3 \left(m_{\mathrm{B}^0} - m_{\mathrm{D}^{*+}}\right)^2 \sqrt{\omega^2 - 1} \times \left[4\omega\left(\omega+1\right)\frac{1-2\omega r + r^2}{\left(1-r\right)^2} + \left(\omega+1\right)^2\right].$$

The unknown function $\mathcal{F}(\omega)$ is approximated with an expansion around $\omega = 1$ [7]:

$$\mathcal{F}(\omega) = \mathcal{F}(1)\left[1 - a^2\left(\omega - 1\right) + b\left(\omega - 1\right)^2\right],$$

where a and b are parameters to be determined by the fit. We use a^2 in the expression for $\mathcal{F}(\omega)$ because the slope of the function is constrained to be negative at $\omega = 1$ [7, 9, 31]. The curvature parameter, b, is not a free parameter but is constrained by the value of a^2. Recent theoretical work suggests it should be $b = 0.66a^2 - 0.11$ [9], which is what we use in the fit.

The detector acceptance and finite ω resolution are taken into account by convolving this distribution with a Gaussian resolution function and an efficiency function, $\epsilon^k(\omega')$:

$$\mathcal{P}_s^k(\omega_i) = \int_1^{\omega_{max}} \frac{1}{I(\omega')} e^{\frac{-(\omega_i - \omega')^2}{2\sigma_\omega^2}} \cdot \frac{1}{J^k} \epsilon^k(\omega')\mathcal{K}(\omega')\mathcal{F}^2(\omega')|V_{\mathrm{cb}}|^2\,\mathrm{d}\omega',$$

where σ_ω is the estimated error on the measured ω and ω_{max} is the maximum value of ω (about 1.50). For 3-prong candidates we use $\sigma_\omega = 0.10$ and for satellite candidates we use $\sigma_\omega = 0.12$. The efficiency is relatively constant as a function of ω, as can be seen in Figure 3. We parameterize it by a linear function. The quantities $I(\omega')$ and J^k are normalization factors:

$$\begin{aligned} I(\omega') &= \int_1^{\omega_{max}} e^{\frac{-(\omega' - \omega)^2}{2\sigma_\omega^2}}\,\mathrm{d}\omega\,, \\ J^k &= \int_1^{\omega_{max}} \epsilon^k(\omega')\mathcal{K}(\omega')\mathcal{F}^2(\omega')|V_{\mathrm{cb}}|^2\,\mathrm{d}\omega'\,. \end{aligned}$$

The normalization factor $I(\omega')$ takes into account that the reconstructed ω is constrained to lie within the physical region.

The reconstructed ω distributions for Monte Carlo simulated background events are used to parameterize the background probability density functions, $\mathcal{P}_b^k$. For the combinatorial background, we use events in the δ_M sideband region, $0.17 < \delta_M < 0.23$ GeV for the 3-prong and $0.18 < \delta_M < 0.23$ GeV for the satellite.

The estimated number of signal events of type k is defined as:

$$N_s^k(a, b, \mathcal{F}(1)|V_{\rm cb}|) = 4N_{mh}\, R_{\rm b} f({\rm b} \to \overline{\rm B}^0)\, \tau_{\rm B^0}\, Br({\rm D}^{*+} \to {\rm D}^0\pi^+)\, J^k\, \mathcal{R}^k, \tag{4}$$

where N_{mh} is the background subtracted, efficiency corrected number of multihadronic $\rm Z^0$ decays used in the analysis, $\mathcal{R}^k = Br({\rm D}^0 \to {\rm K}^-\pi^+)$ for 3-prong candidates and $\mathcal{R}^k = Br({\rm D}^0 \to {\rm K}^-\pi^+\pi^0)$ for satellite events and $\tau_{\rm B^0}$ is the $\rm B^0$ lifetime. We use a value of $\tau_{\rm B^0} = 1.56 \pm 0.06$ ps [28]. The factor of 4 comes from two b quarks per event and two lepton species. The overall likelihood for the sample is

$$\mathcal{L}(a, b, \mathcal{F}(1)|V_{\rm cb}|) = \prod_k P(N_0^k, N_s^k) \prod_{i=1}^{N^k} \mathcal{P}^k(\omega_i)\,, \tag{5}$$

where $P(N_0^k, N_s^k)$ is the Gaussian probability to observe N_0^k signal events (the measured number of signal events) when N_s^k are expected.

Maximizing the likelihood of equation 5 with respect to $\mathcal{F}(1)|V_{\rm cb}|$ and a, we find

$$\begin{aligned} \mathcal{F}(1)|V_{\rm cb}| &= (32.8 \pm 1.9) \times 10^{-3}, \\ a^2 &= 0.55 \pm 0.24\,. \end{aligned}$$

where the errors are statistical only. The correlation between the two quantities is 97%. The distribution of reconstructed ω for the selected ${\rm D}^{*+}\ell^-$ candidates is shown in Figure 4.

For comparison with some of the earlier results [10], [11], [13], where b was ignored altogether, we repeated the fit assuming a linear form, $\mathcal{F}(\omega) = \mathcal{F}(1)\,[1 - a^2\,(\omega - 1)]$. The result of this fit is

$$\begin{aligned} \mathcal{F}(1)|V_{\rm cb}| &= (32.5 \pm 1.7) \times 10^{-3}, \\ a^2 &= 0.42 \pm 0.17\,. \end{aligned}$$

The result is consistent with the value from the constrained quadratic fit.

We further determine the exclusive semileptonic branching fraction from the observed number of signal events, according to the formula

$$Br(\overline{\rm B}^0 \to {\rm D}^{*+}\ell^-\overline{\nu}_\ell) = \frac{N_0^k}{4N_{mh}\, R_{\rm b} f({\rm b} \to \overline{\rm B}^0)\, Br({\rm D}^{*+} \to {\rm D}^0\pi^+)\, \mathcal{R}^k\, \epsilon_0^k}\,,$$

where ϵ_0^k is the total efficiency, integrated over ω, for the 3-prong or satellite sample. The branching fraction is calculated separately for the two modes and then combined to obtain

$$Br(\overline{\rm B}^0 \to {\rm D}^{*+}\ell^-\overline{\nu}_\ell) = (5.08 \pm 0.21)\%\,,$$

where the error is statistical only. This result is in good agreement with recent, precise measurements [11]-[13].

7 Systematic Uncertainties

Systematic uncertainties arise from imprecise knowledge of the background levels in the selected sample as well as uncertainties in the Monte Carlo simulations. The following sources of systematic error have been considered and are summarized in Table 3.

Source of Uncertainty	$\Delta\mathcal{F}(1)\lvert V_{\rm cb}\rvert/\mathcal{F}(1)\lvert V_{\rm cb}\rvert$ (%)	Δa^2	$\Delta Br/Br$ (%)
$R_{\rm b}$	0.5	-	1.0
$f({\rm b}\to\overline{\rm B}^0)$	2.9	-	5.8
$Br({\rm D}^{*+}\to{\rm D}^0\pi^+)$	1.0	-	2.0
$Br({\rm D}^0\to{\rm K}^-\pi^+)$	0.4	0.013	1.2
$Br({\rm D}^0\to{\rm K}^-\pi^+\pi^0)$	2.6	0.026	4.0
$\tau_{{\rm B}^0}$	1.8	-	3.8
$Br(\overline{\rm B}\to{\rm D}^{*+}{\rm h}\ell^-\overline{\nu}_\ell)$	3.6	0.017	7.9
$Br(\overline{\rm B}^0\to{\rm D}^{*+}\tau^-\overline{\nu}_\tau)$	0.4	0.011	0.7
$Br(\overline{\rm B}^0\to{\rm D}^{*+}{\rm D}_{\rm s}^{(*)-})$	0.2	-	0.4
Combinatorial Background	1.2	0.011	1.9
Fake Leptons	0.2	-	0.5
Fake $\rm D^0$	0.5	0.005	1.0
ω Resolution	1.4	0.037	-
Selection Efficiency	2.9	0.006	5.7
Total	6.7	0.052	13.0

Table 3: Summary of systematic uncertainties in the measurement of $\mathcal{F}(1)|V_{\rm cb}|$.

- **Branching fractions and $\mathbf{B^0}$ lifetime:** The quantities $R_{\rm b}$, $f({\rm b}\to\overline{\rm B}^0)$, $Br({\rm D}^{*+}\to{\rm D}^0\pi^-)$, $Br({\rm D}^0\to{\rm K}^-\pi^+)$ and $\tau_{{\rm B}^0}$ are used in equation 4 to predict the number of expected signal events. They were varied within the errors quoted in Table 1 and the fit was repeated. The overall systematic uncertainty, from these sources, on $\mathcal{F}(1)|V_{\rm cb}|$ is 4.4%, which is dominated by the error on $f({\rm b}\to\overline{\rm B}^0)$.
- **Background Estimates:** The size of each background listed in Table 2 was varied by its quoted uncertainty. The uncertainties in the background levels have a contribution from finite Monte Carlo statistics, but are dominated by the errors in the measured branching fractions. The contributions to the uncertainties from $R_{\rm b}$, $f({\rm b}\to\overline{\rm B}^0)$ and the $\rm D^0$ and $\rm D^{*+}$ branching fractions are negligible. The largest systematic error is from the uncertainty in the contribution from $\overline{\rm B}\to{\rm D}^{*+}{\rm h}\ell^-\overline{\nu}_\ell$, which amounts to 3.6% on $\mathcal{F}(1)|V_{\rm cb}|$.
- **Resolution of $\boldsymbol{\omega}$:** For the fit, we assumed an average ω resolution of $\sigma_\omega = 0.10$ for the 3-prong events and $\sigma_\omega = 0.12$ for the satellite events, which are the predictions from the

Monte Carlo simulation. We estimated the uncertainty on the resolution by comparing relevant quantities from data with the predictions from Monte Carlo simulations and propagating any discrepancies into the uncertainty on ω. The resolution on the neutrino direction can be estimated from data by comparing the calculated θ_ν from equation 3 with the value obtained from the reconstructed neutrino direction. We find good agreement between the distribution from data and that predicted from Monte Carlo simulations. We attribute a systematic uncertainty of 10% on σ_ω from this source. From comparisons of missing energy distributions in real data and Monte Carlo simulated events, we estimate an additional 5% on σ_ω from uncertainties in the Monte Carlo modelling of the resolution of E_ν. Adding these uncertainties in quadrature, we estimate an overall systematic uncertainty of 12% on σ_ω. When varying σ_ω by 12%, we observe a 1.4% variation in $\mathcal{F}(1)|V_{\mathrm{cb}}|$. To check our sensitivity to the shape of the resolution function the fit was repeated for two different cases. For the first case, the resolution was parameterized by the sum of two Gaussians. For the second case, we parameterized the resolution separately for five different ω ranges, for which we observed variations of (5-10)% from the mean σ_ω values used in the nominal fit. In both cases, we observed negligible variation in the fitted values of $\mathcal{F}(1)|V_{\mathrm{cb}}|$ and a^2.

- **Selection efficiency:** Systematic uncertainties arise from our $\mathrm{D}^{*+}\ell^-$ selection cuts due to finite Monte Carlo statistics and uncertainties in the Monte Carlo modelling of quantities on which we make cuts [32]. The dominant effects are from uncertainties in the lepton and B meson momentum spectra, which have been investigated in detail in [32]. The uncertainties in the overall efficiencies for the 3-prong and satellite modes translate into a systematic uncertainty of 2.8% on $\mathcal{F}(1)|V_{\mathrm{cb}}|$. We also used alternative parameterizations of the efficiencies as a function of ω, including flat efficiencies, quadratic dependences and bin-by-bin dependences (from figure 3). The resulting variation in $\mathcal{F}(1)|V_{\mathrm{cb}}|$ is 0.9%. Adding in quadrature these two errors, we estimate a total uncertainty of 2.9% on $\mathcal{F}(1)|V_{\mathrm{cb}}|$.

8 Summary and Conclusion

The CKM matrix element $|V_{\mathrm{cb}}|$ has been measured by studying the rate of the exclusive semileptonic decay $\overline{\mathrm{B}}^0 \to \mathrm{D}^{*+}\ell^-\overline{\nu}_\ell$ as a function of the recoil kinematics of the D^{*+} meson. Heavy Quark Effective Theory provides a description of the decay rate in terms of a single hadronic form factor, $\mathcal{F}(\omega)$. Although the shape of the form factor is not specified, its value at $\omega = 1$ can be accurately calculated with little model dependence. Recent theoretical calculations make use of a power series expansion of $\mathcal{F}(\omega)$ around $\omega = 1$, retaining terms up to order ω^2: $\mathcal{F}(\omega) = \mathcal{F}(1)\left[1 - a^2(\omega - 1) + b(\omega - 1)^2\right]$, where the slope is constrained to be negative and the curvature is related to the slope according to the expression $b = 0.66a^2 - 0.11$ [9].

The quantities $\mathcal{F}(1)|V_{\mathrm{cb}}|$ and a^2 are extracted by comparing the measured $\mathrm{d}\Gamma/\mathrm{d}\omega$ spectrum of 1251 ± 125 reconstructed $\overline{\mathrm{B}}^0 \to \mathrm{D}^{*+}\ell^-\overline{\nu}_\ell$ events with the theoretical prediction and extrapolating to $\omega = 1$, where the decay rate vanishes. We find

$$\begin{aligned}
\mathcal{F}(1)\,|V_{\rm cb}| &= [32.8 \pm 1.9\,({\rm stat}) \pm 2.2\,({\rm syst})] \times 10^{-3}, \\
a^2 &= 0.55 \pm 0.24\,({\rm stat}) \pm 0.05\,({\rm syst})\ , \\
Br\left(\overline{\rm B}^0 \to {\rm D}^{*+}\ell^-\overline{\nu}_\ell\right) &= (5.08 \pm 0.21\,({\rm stat}) \pm 0.66\,({\rm syst}))\,\%\,.
\end{aligned}$$

These measurement are consistent with previous results and are of comparable precision [10]-[13].

Using the theoretical estimate $\mathcal{F}(1) = 0.91 \pm 0.03$ [9], we determine

$$|V_{\rm cb}| = [36.0 \pm 2.1\,({\rm stat}) \pm 2.4\,({\rm syst}) \pm 1.2\,({\rm theory})] \times 10^{-3}.$$

Acknowledgements

We particularly wish to thank the SL Division for the efficient operation of the LEP accelerator and for their continuing close cooperation with our experimental group. In addition to the support staff at our own institutions we are pleased to acknowledge the
Department of Energy, USA,
National Science Foundation, USA,
Particle Physics and Astronomy Research Council, UK,
Natural Sciences and Engineering Research Council, Canada,
Israel Science Foundation, administered by the Israel Academy of Science and Humanities,
Minerva Gesellschaft,
Japanese Ministry of Education, Science and Culture (the Monbusho) and a grant under the Monbusho International Science Research Program,
German Israeli Bi-national Science Foundation (GIF),
Direction des Sciences de la Matière du Commissariat à l'Energie Atomique, France,
Bundesministerium für Bildung, Wissenschaft, Forschung und Technologie, Germany,
National Research Council of Canada,
Hungarian Foundation for Scientific Research, OTKA T-016660, and OTKA F-015089.

References

[1] See, for instance, M. Neubert, Int. J. Mod. Phys. **A 11** (1996) 4173.

[2] I. I. Bigi, N. G. Uraltsev and A. I. Vainshtein, Phys. Lett. **B 293** (1992) 430;
I. I. Bigi, M. A. Shifman, N. G. Uraltsev and A. I. Vainshtein, Phys. Rev. Lett. **71** (1993) 496;
B. Blok, L. Loyrakh, M. A. Shifman and A. I. Vainshtein, Phys. Rev. **D 49** (1994) 3356;
A. V. Manohar and M. B. Wise, Phys. Rev. **D 49** (1994) 1310.

[3] For a recent review of HQET see M. Neubert, Phys. Rep. **245** (1994) 259.

[4] M. A. Shifman and M. B. Voloshin, Sov. J. Nucl. Phys. **47** (1988) 511.

[5] N. Isgur and M. Wise, Phys. Lett. **B 232** (1989) 113;
N. Isgur and M. Wise, Phys. Lett. **B 237** (1990) 527.

[6] A. F. Falk, H. Georgi, B. Grinstein and M. B. Wise, Nucl. Phys. **B 343** (1990) 1.

[7] M. Neubert, Phys. Lett. **B 264** (1991) 455;
M. Neubert, Phys. Lett. **B 338** (1994) 84.

[8] M. Luke, Phys. Lett. **B 252** (1990) 447.

[9] I. Caprini and M. Neubert, Phys. Lett. **B 380** (1996) 376.
This paper computes $\mathcal{F}(1)$ using measurements in reference [7] as well as the following:
A. F. Falk and M. Neubert, Phys. Rev. **D 47** (1993) 2965 and 2982;
T. Mannel, Phys. Rev. **D 50** (1994) 428;
M. A. Shifman, N. G. Uraltsev and A. I. Vainshtein, Phys. Rev. **D 51** (1995) 2217;
A. Czarnecki, Phys. Rev. Lett. **76** (1996) 4124.

[10] ARGUS Collaboration, H. Albrecht *et al.*, Z. Phys. **C 57** (1993) 533.

[11] CLEO Collaboration, B. Barish *et al.*, Phys. Rev **D 51** (1995) 1014.

[12] ALEPH Collaboration, B. Buskulic *et al.*, Phys. Lett. **B 359** (1995) 236;
ALEPH Collaboration, B. Buskulic *et al.*, CERN-PPE/96-150, submitted to Phys. Lett. **B**.

[13] DELPHI Collaboration, P. Abreu *et al.*, Z. Phys. **C 71** (1996) 539.

[14] OPAL Collaboration, K. Ahmet *et al.*, Nucl. Instrum. Methods **A 305** (1991) 275.

[15] P. P. Allport *et al.*, Nucl. Instrum. Methods **A 324** (1993) 34;
P. P. Allport *et al.*, Nucl. Instrum. Methods **A 346** (1994) 476.

[16] OPAL Collaboration, G. Alexander *et al.*, Z. Phys. **C 52** (1991) 175.

[17] JADE Collaboration, W. Bartel *et al.*, Z. Phys. **C 33** (1986) 23;
JADE Collaboration, S. Bethke *et al.*, Phys. Lett. **B 213** (1988) 235.

[18] T. Sjöstrand, Comp. Phys. Comm. **39** (1986) 347;
T. Sjöstrand and M. Bengtsson, Comp. Phys. Comm. **43** (1987) 367;
T. Sjöstrand, CERN-TH.6488/92.
The JETSET 7.4 parameters were tuned as described in
OPAL Collaboration, G. Alexander *et al.*, Z. Phys. **C 69** (1995) 543.

[19] J. Allison *et al.*, Nucl. Instrum. Methods **A 317** (1992) 47;

[20] OPAL Collaboration, G. Alexander *et al.*, Z. Phys. **C 70** (1996) 357.

[21] OPAL Collaboration, P. D. Acton *et al.*, Z. Phys. **C 58** (1993) 523.

[22] OPAL Collaboration, R. Akers *et al.*, Z. Phys. **C 65** (1995) 17.

[23] OPAL Collaboration, G. Alexander *et al.*, CERN-PPE/96-101, submitted to Z. Phys. **C**.

[24] OPAL Collaboration, R. Akers *et al.*, Z. Phys. **C 67** (1995) 27.

[25] OPAL Collaboration, R. Akers *et al.*, Z. Phys. **C 66** (1995) 555.

[26] OPAL Collaboration, M. Z. Akrawy *et al.*, Phys. Lett. **B 236** (1990) 224.

[27] ALEPH Collaboration, D. Buskulic *et al.*, Phys. Lett. **B 345** (1994) 103.

[28] Particle Data Group, R. M. Barnett *et al.*, Phys. Rev. **D 54** (1996), Part I *Meson Full Listings.*

[29] LEP Experiments, Nucl. Instrum. Methods **A 378** (1996) 101.

[30] ALEPH Collaboration, D. Buskulic *et al.*, Phys. Lett. **B 343** (1995) 444.

[31] M. Neubert, preprint CERN-TH/95-307 (1995). To be published in the proceedings of the International Symposium on Lepton-Photon Interactions (IHEP), Beijing, China, 10-15 Aug. 1995.

[32] OPAL Collaboration, R. Akers *et al.*, Z. Phys. **C 67** (1995) 57.

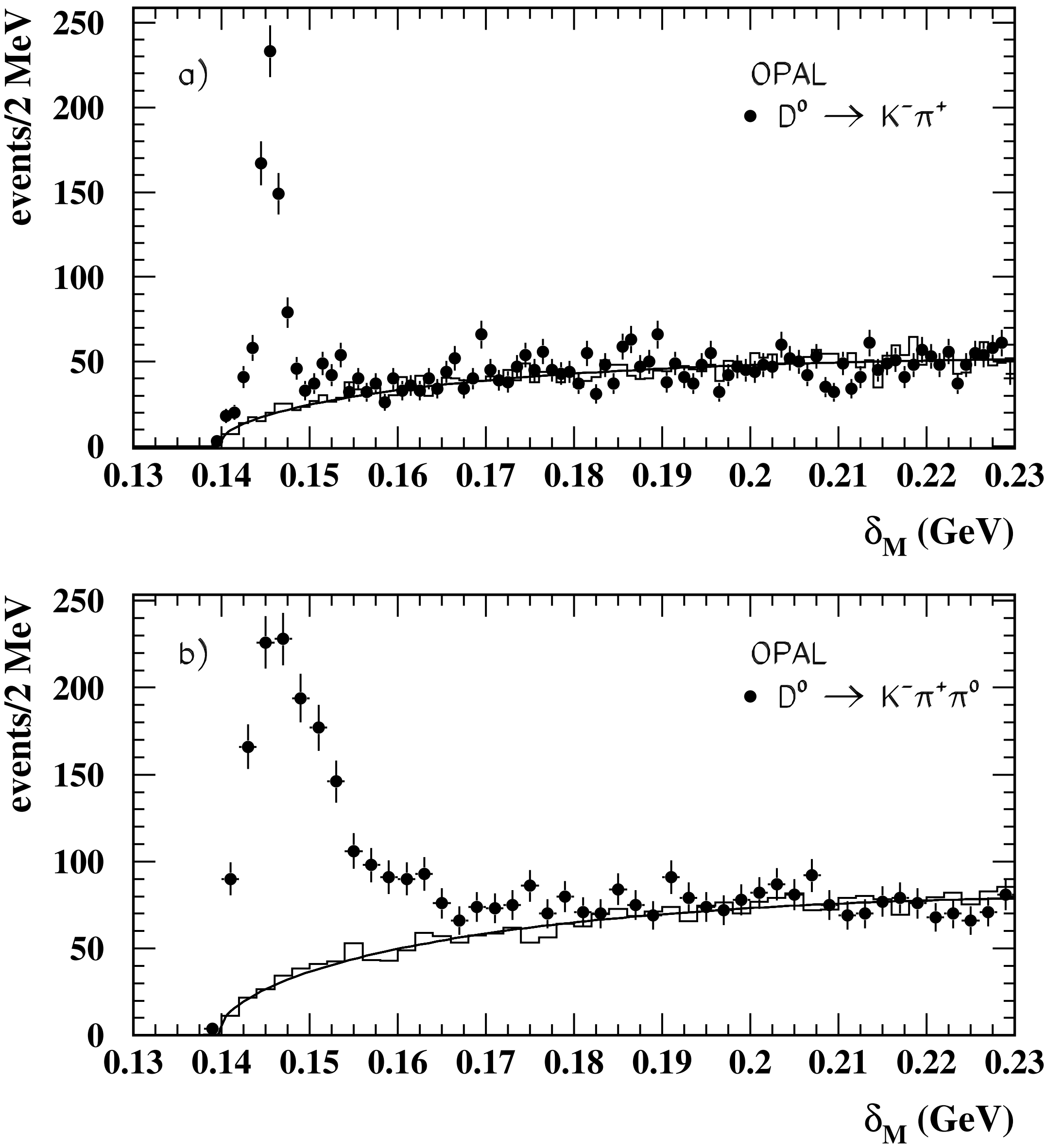

Figure 1: Mass difference between the D^{*+} and D^0 candidates, δ_M, for selected $D^{*+}\ell^-$ events: a) $D^0 \rightarrow K^-\pi^+$ events, b) $D^0 \rightarrow K^-\pi^+\pi^0$ events. The solid curves are the estimated background shapes and the solid histograms represent the normalized reflected pion and wrong sign events.

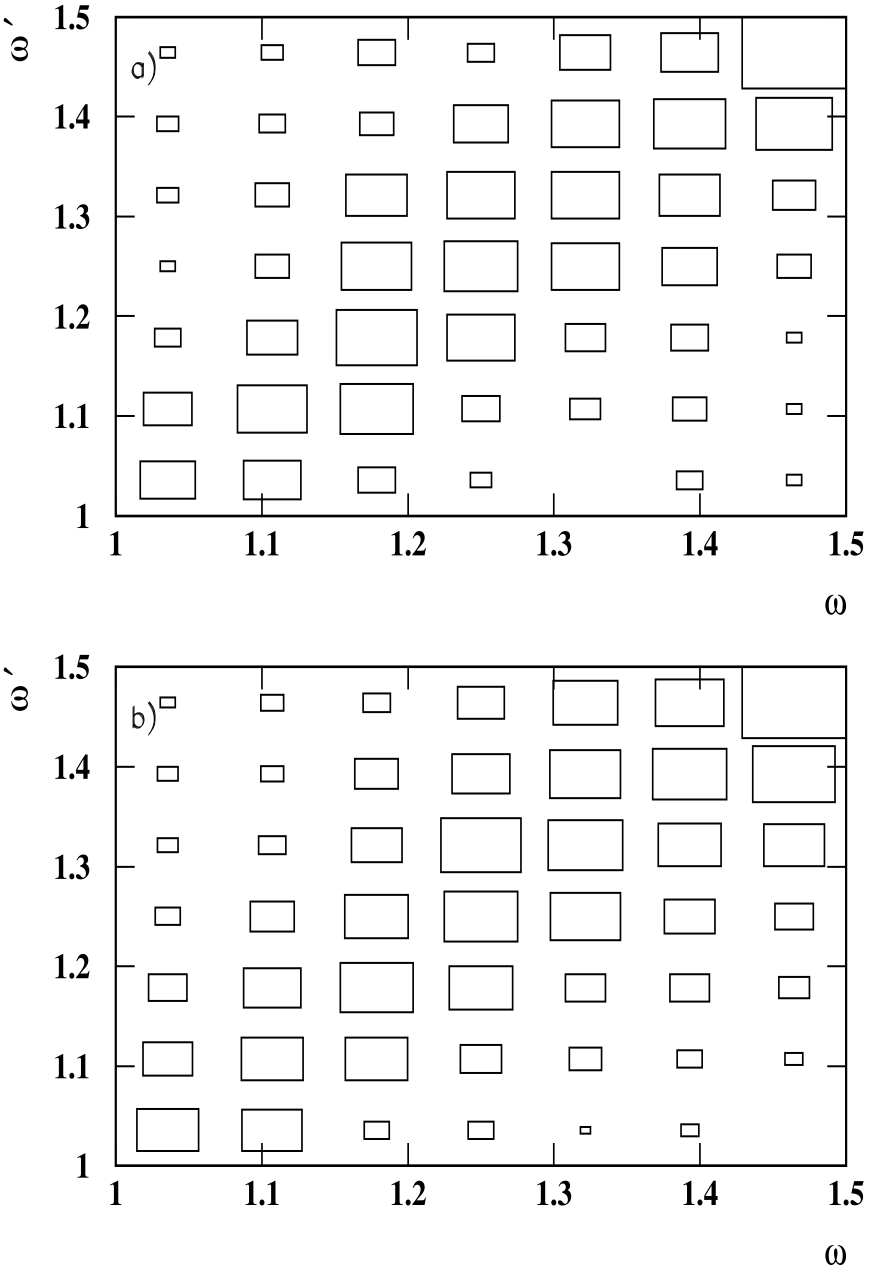

Figure 2: The true value ω' versus the reconstructed value ω for simulated $\overline{B}^0 \to D^{*+}\ell^-\overline{\nu}_\ell$ decays: a) $D^0 \to K^-\pi^+$ events, b) $D^0 \to K^-\pi^+\pi^0$ events. The area of each box is proportional to the number of entries.

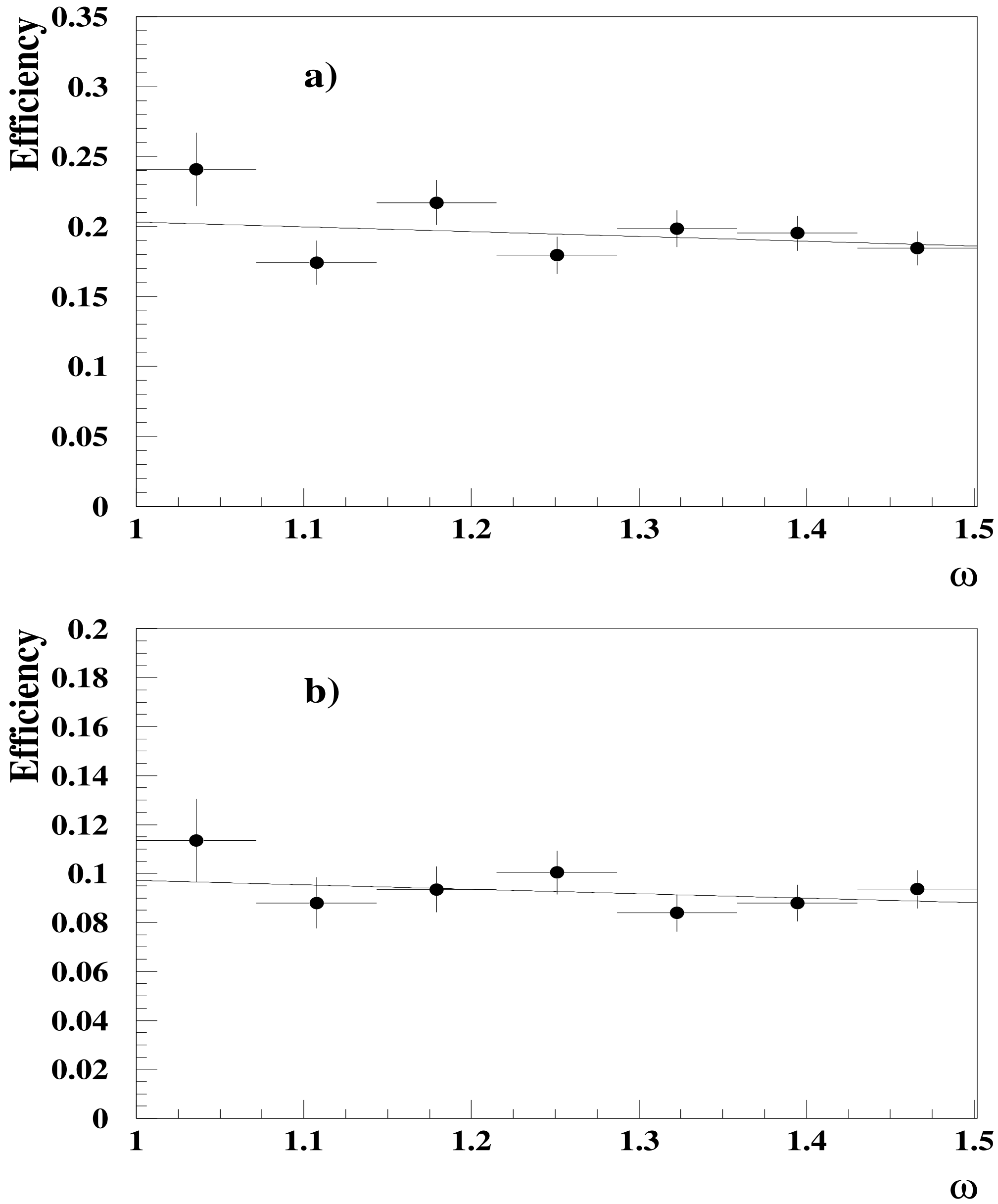

Figure 3: The efficiency as a function of true ω for Monte Carlo simulated $\overline{B}^0 \to D^{*+}\ell^-\overline{\nu}_\ell$ decays: a) $D^0 \to K^-\pi^+$ events, b) $D^0 \to K^-\pi^+\pi^0$ events. The lines are linear fits to the distributions.

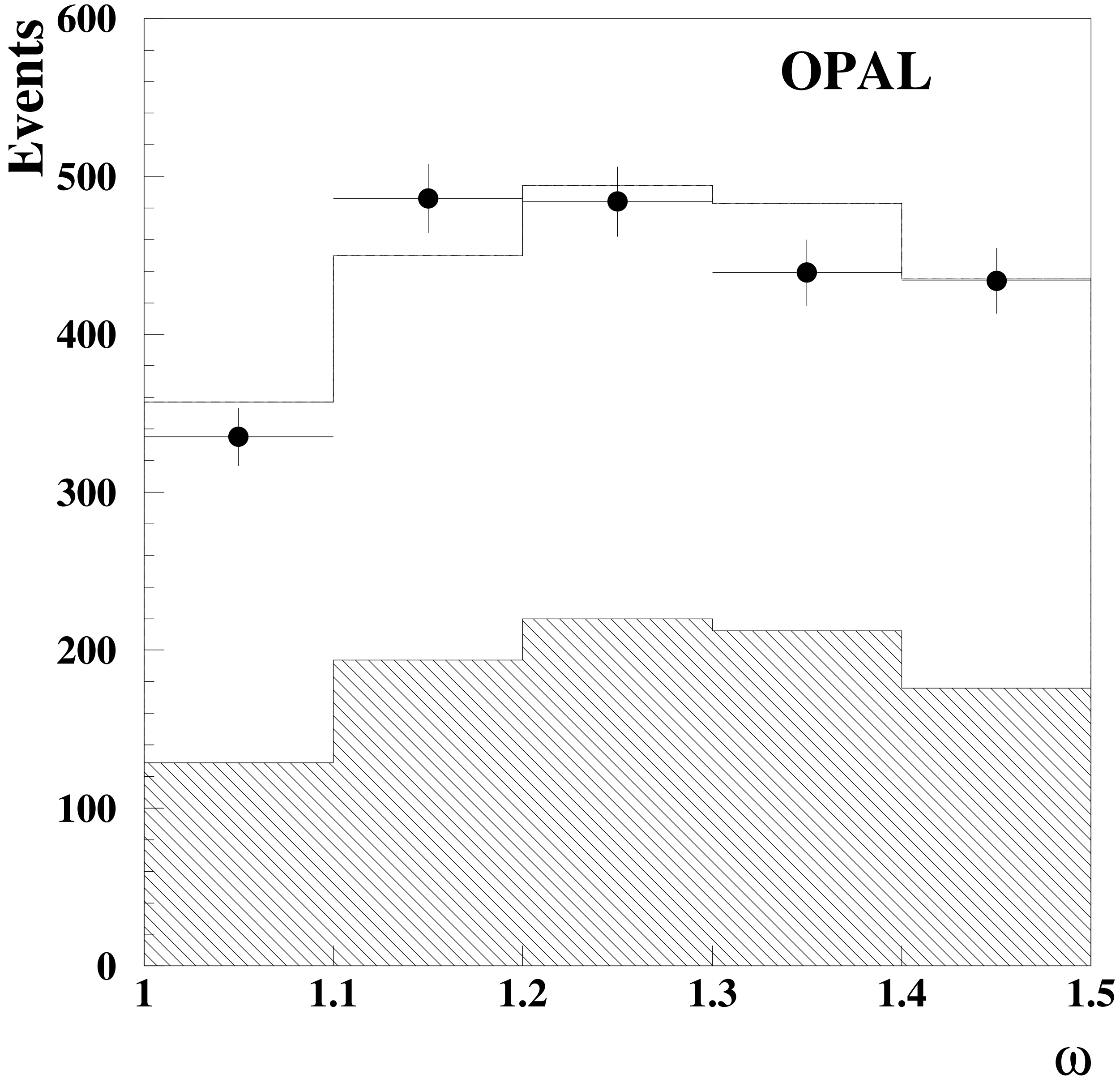

Figure 4: The distribution of reconstructed ω for selected $D^{*+}\ell^-$ candidates. The points are the data, the open histogram is the predicted shape from the fit, including signal and background, and the hatched histogram is the predicted background shape. The error bars on the data points are statistical only.